JOURNAL OF AIRCRAFT
Vol. 45, No. 4, July–August 2008

Experimental Investigation of Lift Enhancement and Roll Control Using Plasma Actuators

Alexander N. Vorobiev,* R. Mark Rennie,† and Eric J. Jumper‡
University of Notre Dame, Notre Dame, Indiana 46556
and
Thomas. E. McLaughlin§
U.S. Air Force Academy, USAF Academy, Colorado 80840

DOI: 10.2514/1.34659

An experimental investigation into the use of trailing-edge-mounted plasma actuators for lift enhancement and roll control is described. Data are presented showing the effect that the actuators have on lift, pitch, and roll moment coefficients as a function of angle of attack and wind speed. The results indicate that the performance of the actuators is strongly influenced by Reynolds number effects. The implications of the findings on the utility of plasma actuators as lift and roll-control devices are discussed.

Nomenclature

α	=	angle of attack
α_{L0}	=	zero-lift angle of attack
b	=	wing span
C_L	=	wing lift coefficient
C_l	=	section lift
C_M	=	wing quarter-chord pitch moment coefficient (M_P/qSc)
C_R	=	wing roll moment coefficient (M_R/qSb)
c	=	wing chord
L	=	lift force
M_P	=	quarter-chord pitch moment
M_R	=	roll moment
P	=	electric power dissipated by the plasma actuator
q	=	dynamic pressure
Re	=	Reynolds number based on chord
S	=	wing planform area
U_∞	=	freestream velocity
x	=	chordwise location on wing or airfoil surface
x_{CP}	=	chordwise location of the center of pressure, nondimensionalized by chord c
y	=	spanwise location on the wing or airfoil surface, from the wing center
y_{CP}	=	spanwise location of the center of pressure, nondimensionalized by half-span $b/2$

I. Introduction

UMANNED aerial vehicles (UAVs) are employed extensively as remote surveillance platforms. Until recently, the expense and size of UAVs has limited their deployment to small numbers and from rear areas. Significant advantage could be gained if the reconnaissance capabilities of UAVs were also made available at the tactical level to small units and forward areas. To satisfy the man-portable requirement of a forward-deployed UAV, new designs incorporating folding or inflatable wings [1,2] are being considered. A serious problem with these designs is that the need to break the aircraft down into a compact storable configuration makes it difficult or impossible to design in conventional control surfaces employing standard mechanical actuators and linkages.

An alternate aerodynamic control technology that shows particular promise is single dielectric barrier discharge devices, or plasma actuators. Consisting of thin, asymmetrically overlapped electrodes separated by a dielectric, the utility of plasma actuators for flow-control applications has been extensively demonstrated [3–7]. When driven by a high-amplitude ac voltage, the electrical discharge formed on the surface of the plasma actuator generates a body force on the surrounding air in the direction of the electrode asymmetry [8,9]. The resulting air jet can be used to, for example, postpone flow separations [3,4] or, more pertinently, to affect aerodynamic forces and moments on a wing [5–7].

Previous attempts to use plasma actuators as lift-enhancement devices are documented in [5]. In these tests, plasma actuators constructed from copper foil electrodes and using a Kapton film dielectric were mounted at the three-quarter-chord location ($x/c = 0.75$) of a 0.2-m chord, 0.417 m wide, end-plated airfoil with the NACA0009 profile. Lift and drag data were acquired as a function of angle of attack and at two wind speeds. These data indicated that the plasma actuators produced a measurable amount of lift enhancement that remained constant as a function of both angle of attack and wind speed. As such, the change in lift coefficient, ΔC_L, produced by the actuators was found to drop off as the square of the wind speed, which appears in the denominator of ΔC_L as part of the nondimensionalizing dynamic pressure term:

$$\Delta C_L \propto \frac{1}{U_\infty^2} \tag{1}$$

The data acquired in [5] were possibly the first of their kind that experimentally demonstrated the ability of plasma actuators to control the lift on an airfoil. Using computational methods, the constant-lift-enhancement results of [5] were shown to be a natural outcome of the constant momentum addition, or body force, that plasma actuators impart to the flow [6,7]. The computational models were calibrated using the experimental data of [5], which were then used to demonstrate that roll moments sufficient to control an airplane should be possible using existing plasma-actuator technology. The purpose of the experimental investigation described

Presented as Paper 3383 at the 37th AIAA Plasmadynamics and Lasers Conference, San Francisco, CA, 5–8 June 2006; received 18 September 2007; revision received 6 March 2008; accepted for publication 7 March 2008.

*Graduate Research Assistant, Center for Flow Physics and Control, Department of Aerospace and Mechanical Engineering. Student Member AIAA.

†Assistant Research Professor, Center for Flow Physics and Control, Department of Aerospace and Mechanical Engineering. Senior Member AIAA.

‡Professor, Center for Flow Physics and Control, Department of Aerospace and Mechanical Engineering. Fellow AIAA.

§Director, Aeronautics Research Center, Department of Aeronautics. Associate Fellow AIAA.

in this article was therefore twofold: to repeat and validate previous lift-enhancement results documented in [5] and to extend those results to the use of plasma actuators as roll-control devices on a three-dimensional wing.

II. Experiment

A. Model

The measurements were made in the Atmospheric Wind Tunnel (AWT) at the Hessert Laboratory of the University of Notre Dame. This wind tunnel is an open-circuit configuration with test-section dimensions of 1.8×1.8 m. The tunnel turbulence-intensity level is less than 2%, and maximum wind speed is approximately 10 m/s.

The wing used for the lift-enhancement investigations was made out of epoxy and had the NACA0009 profile. The wing had a 0.2-m (8-in.) chord and a span of 0.91 m (36 in.), giving it an aspect ratio of 4.5:1. Because the objective was to measure aerodynamic lift and moments in three-dimensional flow, end plates were not used; however, thin 25-mm-wide aluminum bars were attached to the tips of the wing to suspend the wing upside down from a roof-mounted balance system, described next. The angle of attack of the wing was changed by varying the length of the suspending wires, with an estimated accuracy of ± 0.25 deg. Drag force was not measured; rather, the wing was restricted from moving in the streamwise direction by thin steel wires attached to the wing tips at the quarter-chord location. A schematic of the roof-mounted aerodynamic balance system is shown in Fig. 1. A photograph of the wing model mounted in the AWT test section is shown in Fig. 2.

B. Actuators

The plasma actuators were constructed using thin electrodes made of copper foil tape attached to a glass-ceramic dielectric (trade name Macor). This type of dielectric is particularly well suited to plasma-actuator applications because of its superior ability to withstand high plasma discharge powers. A schematic showing the construction of the plasma actuators used in this investigation is shown in Fig. 3a. Further details regarding the construction and operation of plasma actuators can be found in [3–7], and a detailed explanation of the physics behind plasma actuators is contained in [8,9].

Two separate and independently controllable 0.4-mm-wide actuators were installed on the left and right sides of the wing to enable lift enhancement (actuators operated concurrently) and control of the wing roll moment (actuators operated independently). The thickness of the Macor dielectric used in the actuators was 1.8 mm, and the actuators were recessed into the suction side of the wing so that no steps or gaps existed with the actuators installed. The streamwise extent of the actuators was approximately 40 mm and the upstream (exposed) electrodes were situated at $x/c = 0.75$. This location for the plasma actuators was selected based on previous studies [5–7], which showed that aerodynamic force and moment control improves as the actuators are mounted further rearward on the wing; the $x/c = 0.75$ position was the farthest downstream location at which the actuators could be mounted without overly weakening the trailing-edge region of the wing model. The geometry of the actuator installation can be seen in Fig. 2.

Power cables leading from the wing-mounted actuators to amplifying circuitry located outside the test section were loosely hung from the model's wing tips. Measurements of the wing's aerodynamic forces made with the power cables attached and removed showed that the aerodynamic behavior of the wing was not influenced by the presence of the cables.

A diagram of the circuit used to drive the plasma actuators is shown in Fig. 3b. The key element is the 150:1 transformer shown in the center of the diagram that was used to step up the low-level driving signal to the kilovolt levels required by the plasma actuators. The plasma actuators were driven by a positive sawtooth signal [10] with a frequency of 2.9 kHz. The voltage and current of the signal driving the plasma actuators were measured using high-voltage and inductive-current probes. Representative actuator voltage and current time histories over three cycles of excitation are shown in Fig. 4. The mean power dissipated by the actuator was computed for each test condition by integrating the product of the instantaneous voltage and current over 128 cycles:

$$P = \frac{1}{NT}\int_{NT} V(t)I(t)\,\mathrm{d}t, \qquad N = 128 \tag{2}$$

All plasma-on data presented in this paper were acquired using a constant mean dissipated power of 65 W per actuator (130 W total power in experiments with both actuators and 65 W in experiments with a single actuator).

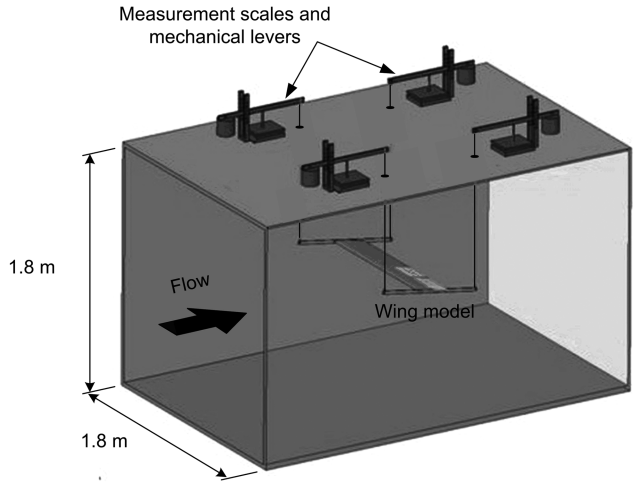

Fig. 1 Schematic of the roof-mounted balance system used for lift and moment measurements on the three-dimensional wing model.

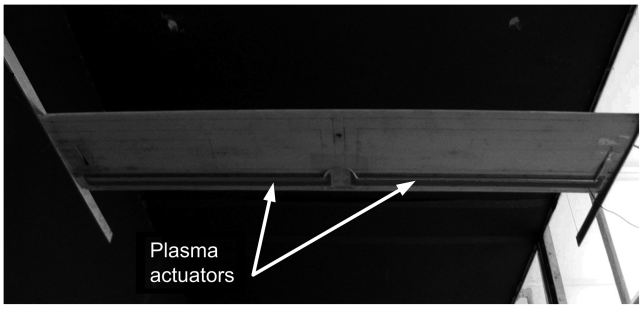

Fig. 2 Photograph of the wing model mounted in the test section of the AWT; flow direction is from top to bottom.

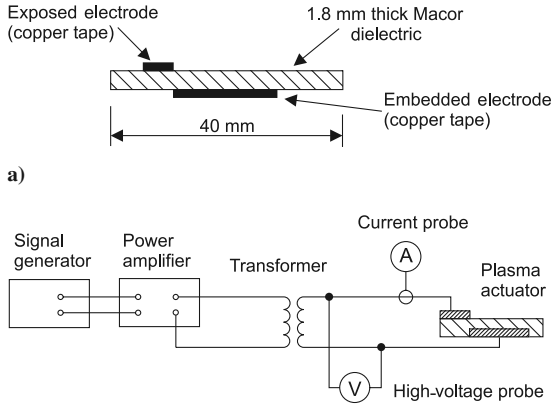

Fig. 3 Diagram of a) plasma actuator and b) power-amplification circuit.

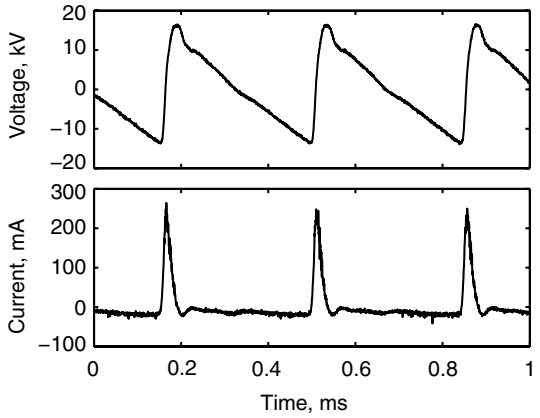

Fig. 4 Representative actuator voltage and current time histories.

C. Data Acquisition and Analysis

Initial tests showed a slight drift in the aerodynamic effect of the plasma actuators during long runs, which was attributed to thermal deformation of the model due to heating by the plasma discharge. As such, measurement sets were acquired by measuring the aerodynamic forces over many short-duration runs, rather than over a single run of longer duration. Each run consisted of a measurement made with the plasma off, followed immediately by one with the plasma on, with the aerodynamic effect of the actuators reported as the difference between the plasma-on and the plasma-off states.

An additional source of measurement error was the radio frequency (RF) noise emitted by the actuators during operation. To minimize the effect of RF noise on the data, a novel force-measurement system was employed using four electronic scales mounted on the roof of the AWT test section (Fig. 1). The scales were specially shielded for operation in high-frequency electromagnetic-noise conditions. Aerodynamic loads acting on the wing were transmitted to the scales by steel wires attached to the aluminum wing-tip-mounted support bars. To increase the signal-to-noise ratio of the force-measurement system, the aerodynamic loads transmitted to the scales were mechanically amplified by a factor of 3 using lever arms. The forces measured by the four scales were resolved into lift, pitch, and roll moments.

Despite efforts to minimize the influence of the plasma discharge on the data-acquisition system, the RF noise of the plasma discharge still created a small offset in the measured forces. The lift increase measured for the plasma actuators therefore consisted of two terms:

$$\Delta L_{\mathrm{RAW}} = \Delta L + \Delta L_{\mathrm{RF}} \tag{3}$$

where the first term is the lift produced by the plasma actuator and the second term is the lift offset produced by the RF noise of the plasma discharge, typically in the range of 0.02 N. The RF noise influence was found to be constant when the plasma power was not changed; as such, this noise-induced offset was accounted for by taring the balances before data acquisition, with the plasma actuators energized and the wind tunnel off.

III. Results

A. Behavior of the NACA0009 Profile

The NACA0009 profile used in the experiments was chosen to enable comparison with results reported in [5], but also because it is a fundamental profile that is simple to manufacture. This profile, however, undergoes considerable and rapid changes in its flow physics at the low Reynolds numbers relevant to small-scale UAVs. The variation in flow physics of the airfoil is readily apparent from oil-flow-visualization measurements that were made at a Reynolds number of $Re = 130,000$ ($U_\infty = 9$ m/s). To reduce end effects and improve the visualization results, the tests were performed using a two-dimensional airfoil model with the same 0.2-m chord length as the three-dimensional wing model. The measurements were performed in a 2×2 ft test section of one of the University of Notre Dame's subsonic wind tunnels and, although the airfoil model was not end-plated, it spanned the full width of the test section. The oil used for the tests was a mixture of kerosene, mineral oil, and fluorescence dye, which fluoresces under ultraviolet illumination.

The oil-flow visualizations showed that at low angles of attack ($\alpha \sim 0$ to 2 deg), the boundary layer on the suction surface is fully laminar and that the airfoil undergoes trailing-edge boundary-layer separation at a location that moves upstream as the angle-of-attack increases. At $\alpha \sim 3$ deg, the flow topology on the airfoil switches to a leading-edge separation bubble that reattaches as a turbulent boundary layer. The suction-surface boundary layer remains turbulent as the angle-of-attack increases until trailing-edge boundary-layer separation occurs rapidly followed by stall at $\alpha \sim 10$ deg. The preceding interpretation of boundary-layer condition (laminar versus turbulent and attached versus separated) in the various flow visualizations conforms to the results of low-Reynolds-number studies in [11,12] and was also confirmed by hot-wire measurements of velocity profiles near the airfoil surface.

Oil-flow patterns on the suction surface of the airfoil that show the flow physics at low ($\alpha = 1.5$ deg) and moderate ($\alpha = 6$ deg) angles of attack are summarized in Fig. 5. The resulting effect of the changing airfoil-flow physics on the airfoil lift curve is included in the figure. To make the variations in lift curve more discernible, the figure includes a linear theoretical lift curve computed using a

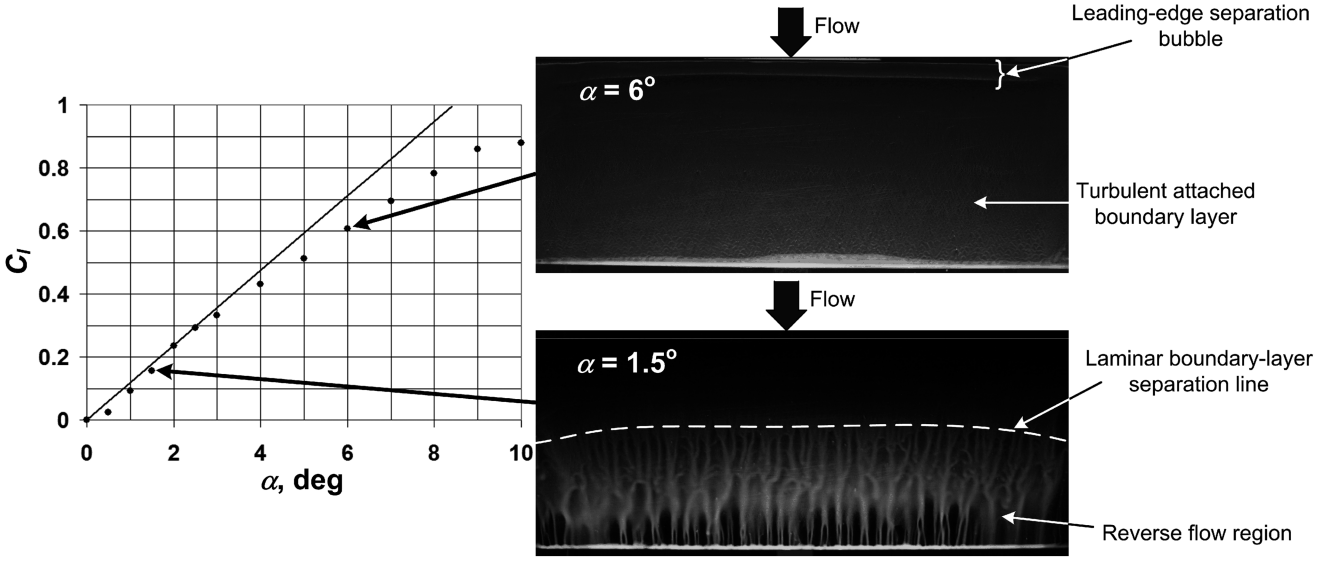

Fig. 5 Lift curve and oil-flow visualizations on the suction surface of the NACA0009 airfoil; $Re = 1.3 \times 10^5$.

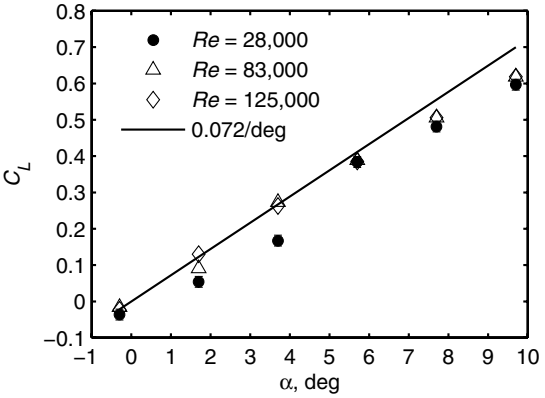

Fig. 6 Lift curve for the wing; plasma actuators are not activated.

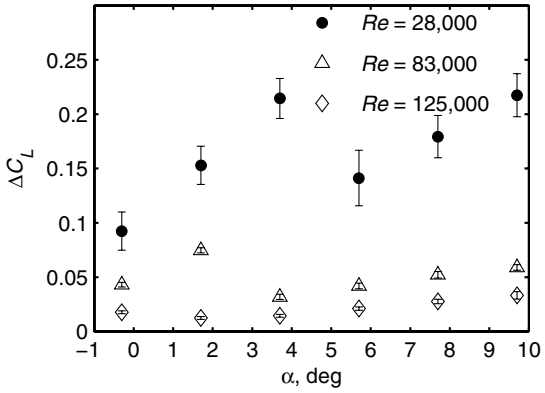

Fig. 7 Lift enhancement with both left and right plasma actuators operating for several Reynolds numbers.

two-dimensional panel method [13]. At angles of attack greater than approximately 4 deg, the wing lift curve exhibits a familiar reduction in lift below the theoretical level that is caused by the increased importance of viscous effects at higher angles of attack: in this case, the thickening of the turbulent boundary layer on the suction surface of the wing. A more unusual feature of the lift curve is the dip in the angle-of-attack region from roughly 0- to 2-deg angle of attack; from the flow-visualization results, this dip corresponds to laminar flow separation on the airfoil suction surface.

Equivalent lift curves for the three-dimensional wing model are given in Fig. 6. The figure includes a theoretical lift curve computed using lifting-line theory [14] that accounts for wind-tunnel blockage effects, giving a theoretical lift–curve slope of $C_{L\alpha} = 0.072/\,\text{deg}$. The similarity between the two- and three-dimensional lift curves indicates that the flow visualizations performed on the two-dimensional airfoil still capture the essential physics of the three-dimensional flow. It is apparent therefore from these baseline flow studies that the trailing-edge-mounted plasma actuators employed with the NACA0009 profile encounter laminar, turbulent, attached, and/or separated boundary-layer flows over the tested angle-of-attack range. All of these flows can be expected to be important to the aerodynamics of small-scale low-Reynolds-number UAVs; as such, the NACA0009 might be considered a fortuitous choice of airfoil because it provides a platform that is suitable for the investigation of the behavior of plasma actuators in effectively all possible flow conditions. As will be shown, the interaction of the plasma actuators with the viscous flowfield of the wing is an important effect determining the performance of the actuators.

B. Lift Enhancement Using Plasma Actuators

Lift-enhancement results for the wing with both left and right actuators operating are shown in Fig. 7 for several values of the chord Reynolds number. As previously described, the data are presented as the change in lift coefficient between the plasma-on and the plasma-off results. The concomitant effect of the actuators on the wing pitch and roll is shown in Fig. 8, which shows the complete effect on aerodynamic forces and moments for a single representative Reynolds number, $Re = 83,000$. As shown in the figures, simultaneous operation of both plasma actuators increased the lift coefficient of the wing at all Reynolds numbers, while imparting a nose-down quarter-chord pitch moment. The fact that the actuators had no discernible effect on the wing roll moment indicates that the lift forces imparted by the left and right actuators were well balanced.

The maximum lift enhancement for the data shown in Fig. 7 corresponds to a lift force of approximately $\Delta L \approx 0.3$ N, which compares well to lift-enhancement values reported in [5]; however, the lift-enhancement results shown in Figs. 7 and 8 show considerable variation over the investigated angle-of-attack range. Figure 8 shows two distinct deviations from constant lift enhancement, consisting of a peak in ΔC_L at an angle of attack of $\alpha = 1.5$ deg and a gradual increase in ΔC_L as the angle of attack increases from around $\alpha = 4$ to 10 deg. These kinds of variations were not observed in results reported in [5], which showed constant

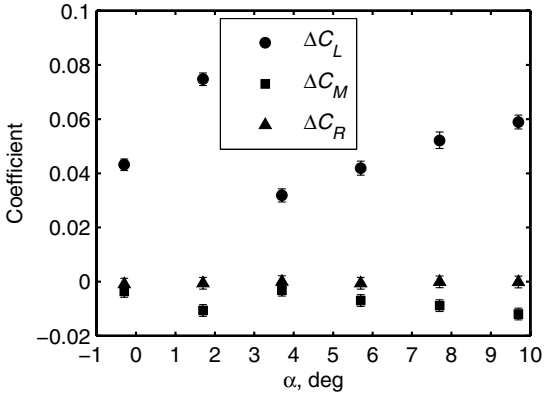

Fig. 8 Changes in aerodynamic forces and moments for a single Reynolds number; $U_\infty = 6.1$ m/s and $Re = 83,000$; both left and right plasma actuators are operating.

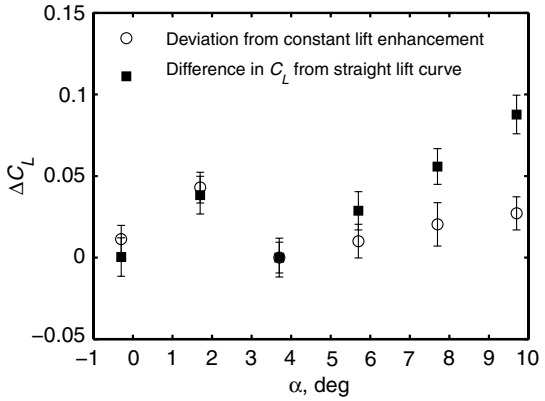

Fig. 9 Comparison of measured variation in lift enhancement with the difference in lift curve from inviscid behavior.

lift enhancement over the same angle-of-attack range. In [5], the lift enhancement was attributed to an increase in airfoil-bound circulation due to the momentum added to the flow by the plasma actuator, which behaved like a wall-bounded jet.

The source of the lift-enhancement variations in Figs. 7 and 8 is indicated by a comparison of the ΔC_L variation in Fig. 8 with the wing lift curve in Fig. 6, which shows an exact angle-of-attack congruence between regions of increased ΔC_L enhancement and regions in which the lift is depressed, due to viscous effects, below the theoretical linear lift curve in Fig. 6. This congruence suggests that the deviations from constant ΔC_L in Fig. 8 are due to the interaction of the plasma actuators with the viscous flowfield of the wing; in effect, the plasma actuators, in addition to increasing the wing's circulation by adding momentum to the flow as reported in

[5], also have an additional flow-control effect in which the actuators counteract depressions in the C_L–α curve by suppressing viscous effects. The absence of a similar flow-control effect of the actuators in the data reported in [5] is likely due to the higher Reynolds numbers that were investigated in [5]. The preceding ideas are more clearly illustrated in Fig. 9, which shows the following:

1) The variation in lift enhancement taken from Fig. 8, computed as the difference between the measured ΔC_L enhancement at each angle of attack and the minimum ΔC_L measured at 3.5-deg angle of attack (circles).

2) The influence of viscous effects on the wing plasma-off lift curve, estimated as the difference at each angle of attack between the straight lifting-line curve and the measured C_L data at the same Reynolds number, taken from Fig. 6 (squares).

The good agreement between the two data sets up to an angle of attack of approximately 6 deg supports the supposition that the plasma actuators elevate the lift closer to the theoretical inviscid limit in this angle-of-attack range. Beyond $\alpha = 6$ deg, the excess lift enhancement is less than the drop-off of C_L from the theoretical lift curve; however, this may simply indicate that the plasma actuators were not powerful enough to fully compensate the reduction in lift due to viscous effects at high angles of attack as the airfoil approaches stall. Similar trends to those shown in Figs. 8 and 9 were observed at all investigated Reynolds numbers.

The effect that the plasma actuators have on the viscous flowfield of the NACA0009 profile is clearly indicated by flow visualizations around the trailing edge. Figures 10a and 10b show smoke-flow-visualization photographs around the trailing edge of the NACA0009 airfoil with the same chord length and with the same plasma actuators shown in Fig. 3 mounted at the same $x/c = 0.75$ location as on the wing. The photographs were taken at a Reynolds number and angle of attack corresponding to the laminar-separation dip in the measured lift curve (Fig. 6). With the plasma actuators turned off (Fig. 10a), the image shows laminar boundary-layer separation upstream of the trailing edge. When the actuators were energized (Fig. 10b), this separated-flow region was eliminated, resulting in a flow that shows a more rigorous enforcement of the airfoil Kutta condition, implying a concomitant increase in the airfoil lift closer to the theoretical limit. These flow-visualization results provide convincing evidence that the plasma actuators, in addition to providing lift enhancement by adding momentum to the flow [5–7], also cause a further increase in the wing lift by effecting a flow-control suppression of the existing viscous flowfield [3,4].

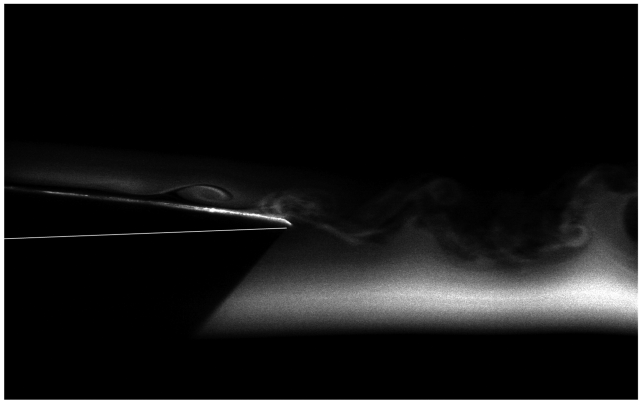

a)

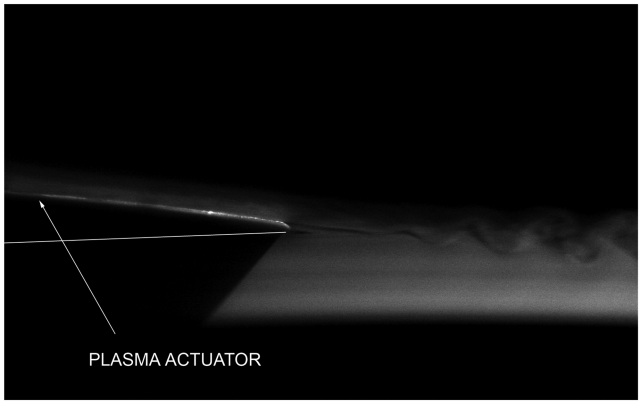

b)

Fig. 10 Visualization of the flow near the trailing edge of the NACA 0009 airfoil: a) plasma off and b) plasma on; $Re = 83,000$ and $\alpha = 2$ deg.

1. *Reynolds Number Dependence*

The plasma-actuator lift enhancement was also measured as a function of wind speed and Reynolds number and is shown in Fig. 11 for three angles of attack. Like the angle-of-attack data shown previously, the data also show significant variation in lift enhancement with changing Reynolds number. The figure shows two distinct variations of the lift enhancement: First, a general drop-off of the lift enhancement to zero occurs as the wind speed decreases to 0 m/s for all angles of attack. Second, at $\alpha = 2$ deg, the lift enhancement undergoes a sudden dip in the wind speed range 6–9 m/s. Because at $\alpha = 2$ deg the wing has large regions of laminar boundary-layer separation, it is likely that the strong Reynolds number variation at this angle of attack is the result of an interaction between the separated-flow region and the plasma flowfield; however, further investigation is required. At angles of attack greater than 4 deg, the lift enhancement asymptotes to a constant value as the wind speed increases to the maximum tested value of 10 m/s.

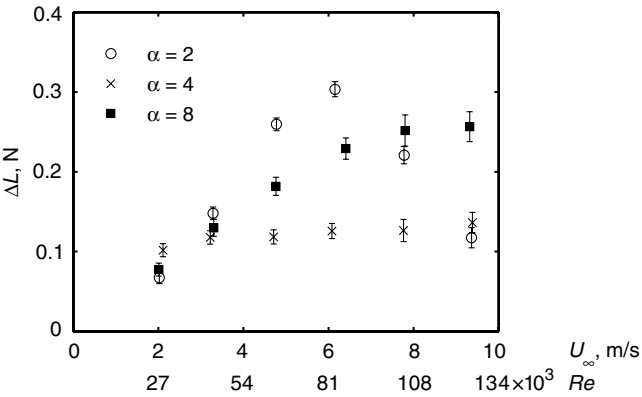

Fig. 11 Variation of lift enhancement with wind speed; both left and right plasma actuators are operating.

2. *Center of Pressure*

The chordwise center of pressure x_{CP} for the lift enhancement was computed from the lift and moment data acquired at all wind speeds. The resulting values for x_{CP} were found to be invariant with wind speed, and the mean location of the center of pressure, averaged over all tested wind speeds, was $x_{CP} \approx 0.40 \pm 0.06$. This location of x_{CP}, rearward of the quarter-chord point, indicates that the plasma actuators produced a noticeable modification to the pressure distribution over the wing. For comparison, the center of pressure of a plain mechanical flap with a hinge line at $x/c = 0.75$ (the location of the upstream electrode of the plasma actuators) is $x_{CP} = 0.71$.

The fact that the plasma actuators produce a rearward shift of the wing loading indicates that the actuators do not behave as simple circulation-enhancement devices. In previous computational investigations [6,7], the effect of the plasma actuators was modeled using a panel method [13] in which the actuators were simulated using a doublet placed at the location of the actuator. The strength of the doublet was calibrated using experimental data, so that constant momentum was injected into the flow at all angles of attack and wind speeds. Results obtained with this method also indicated a rearward loading of the airfoil with plasma actuation; as such, these experimental results confirm the panel-code results and demonstrate

the utility of this kind of panel-code model for investigating plasma-actuator dynamics.

C. Roll Control Using Plasma Actuators

A second objective of the investigation was to evaluate the suitability of plasma actuators for roll control. As previously stated, two independently operable actuators were installed on the wing model, and roll control was achieved by operating one or the other actuator independently (Fig. 12).

A simple illustration of the lift and roll dynamics possible with the wing/actuator system is presented in Fig. 13. The figure shows the measured change in wing lift and roll moment for 4 cases: actuators off, both actuators operated together, and each actuator operated independently. As shown in the figure, for the same test conditions, each actuator produced approximately half the lift enhancement that was gained when both actuators were run together, and each actuator produced an equal but opposite-directed roll moment when operated independently. These results conform to intuitive expectations for the effect of the actuators and show that the two actuators were well balanced in terms of the lift enhancement that they produced. Aerodynamic force coefficients measured during operation of a single actuator are summarized in Figs. 14 and 15. These figures show behavior similar to the two-actuator performance data shown in Figs. 8 and 11.

The location of the wing's spanwise center of pressure, y_{CP}, during single-actuator operation was calculated from the measured lift enhancement and roll moment produced by the actuator. These computations gave a value of $y_{CP} = 0.37$. For comparison, a spanwise location for the center of pressure was also computed using lifting-line theory [14]. For this calculation, the lifting-line equation was solved using a constant value for the zero-lift angle of attack over the spanwise region corresponding to the location of the plasma flap on the experimental model. The resulting lift distribution is plotted in Fig. 16. The spanwise center of pressure for this computed lift distribution is $y_{CP} = 0.35$, which closely matches the preceding experimentally measured value. This result suggests that the plasma actuator gave constant lift enhancement across its spanwise dimension.

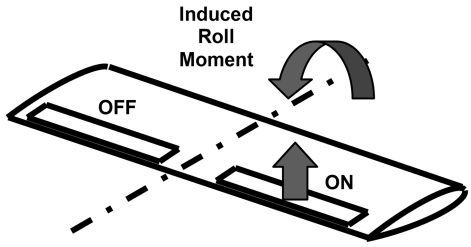

Fig. 12 Roll moment produced by operation of a single actuator.

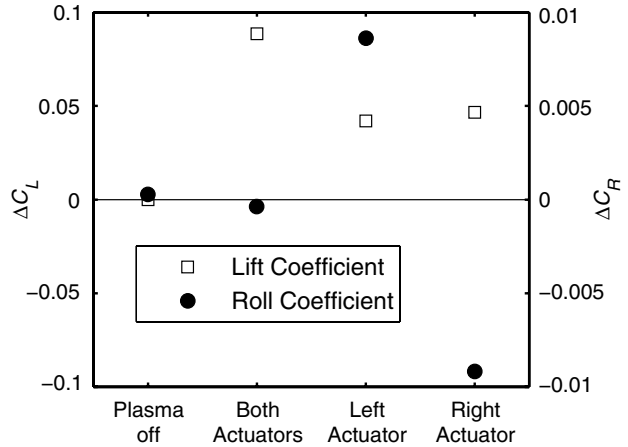

Fig. 13 Example of the lift and roll moments for combined and independent operation of left and right plasma actuators.

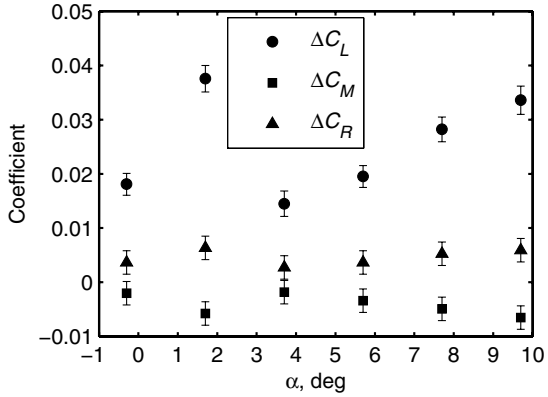

Fig. 14 Changes in aerodynamic forces and moments with a single plasma actuator operating; $U_\infty = 6.1$ m/s and $Re = 83,000$.

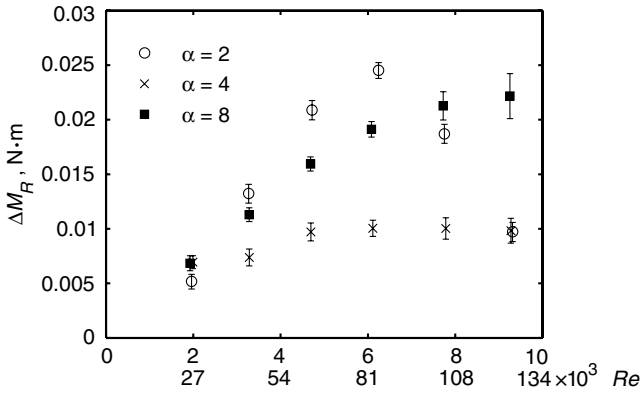

Fig. 15 Roll moment dependence on wind speed and Reynolds number with a single actuator operating; $\alpha = 4$ deg.

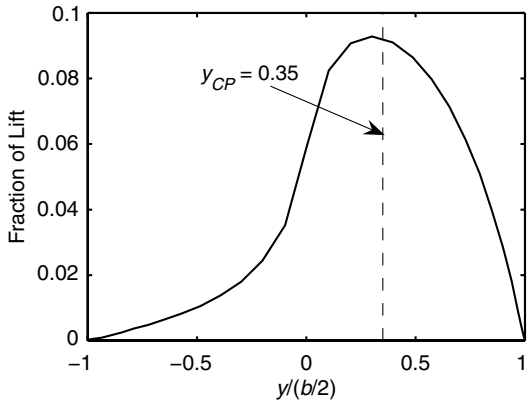

Fig. 16 Lifting-line prediction of lift distribution for constant wing twist over a spanwise distance matching the extent of the right-hand-side plasma actuator.

IV. Discussion and Conclusions

The experimental data acquired in this investigation demonstrate clearly that plasma actuators generate measurable lift enhancement and roll moments on three-dimensional wings and reveal the following trends:

1) The actuators can have a dual effect on the wing lift, consisting of an increase in wing circulation via an inviscid addition of momentum to the flow, and a flow-control suppression of viscous effects near the trailing edge that increases the wing lift via a more rigorous enforcement of the Kutta condition.

2) The fact that the actuators generate a nose-down pitch moment, in addition to lift enhancement, implies that the actuators produce an increase in the rearward load distribution of the wing.

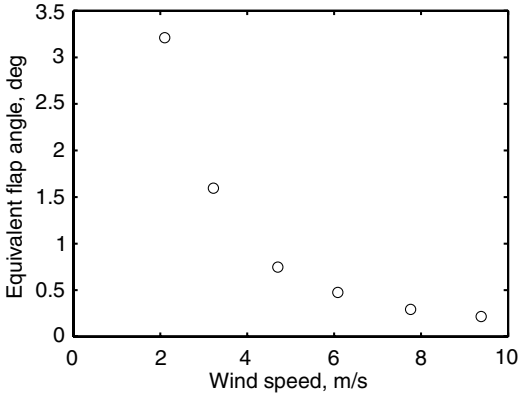

Fig. 17 Equivalent plain flap deflection angles to generate lift enhancement similar to that measured with the plasma actuators used in this investigation ($P = 130$ W); $\alpha = 4$ deg.

3) The actuators generate constant lift enhancement across their span.

The data were acquired at significantly lower Reynolds numbers than those reported in [5] that are relevant to the aerodynamics of man-portable UAVs. In particular, the data have shown that large variations in the lift enhancement of the plasma actuators can exist at low Reynolds numbers. Although further investigation is necessary, several possible explanations can be advanced for the low-Reynolds-number dependence of the lift enhancement shown in Fig. 11. First, the drop-off in ΔL as the wind speed approaches zero may be an inviscid-flow effect that represents a transition region between the zero lift that an actuator must produce at zero freestream velocity and the full lift enhancement that occurs at high wind speed, or the drop-off region may be a viscous-flow effect, caused by typical Reynolds number effects such as a thick or separated boundary layer at the location of the plasma actuator. Second, the dip in ΔL in the $\alpha = 2$ deg data is likely caused by an interaction of the actuator with the unusual low-Reynolds-number behavior of the airfoil in the range of $\alpha = 1$ to 4 deg: for example, a positioning of the laminar boundary-layer separation point close to the location of the plasma actuator. Further measurements are necessary to investigate these findings.

To conclude this section, an indication of the effectiveness of the plasma actuators as lift-enhancement devices was generated by computing equivalent flap deflection angles that produce the same ΔC_L as that measured for the plasma actuators used in this investigation. The equivalent flap angles were estimated using lifting-line theory to determine, in a trial-and-error fashion, the α_{L0} value for an equivalent-span wing twist that produces the same ΔC_L as that measured in the experiment. These α_{L0} values were then used to compute corresponding flap deflection angles using linear airfoil theory with the location of the equivalent flap hinge line arbitrarily defined to be at the same location as the upstream actuator electrode, $x/c = 0.75$.

The results of these calculations are summarized in Fig. 17, which shows equivalent flap angles ranging from around 3 deg at low wind speed, falling to a fraction of a degree at the maximum tested wind speed of 10 m/s. The fall off in equivalent flap angle is due to the fact that the plasma actuators asymptote to a constant lift enhancement (for angles of attack outside the 1- to 4-deg trailing-edge separation region), as opposed to the constant lift coefficient produced by a flap. Aircraft dynamics are determined, however, by dimensional forces and moments; the constant roll moment produced by plasma actuators simply means that they will produce, to first order, the same roll rate regardless of wind speed. In this regard, plasma actuators may offer some advantage over flapped control surfaces, in that the designer may be able to employ simpler control systems if the same roll moment can be expected every time the actuators are energized. The results shown in Fig. 17 should be regarded as order-of-magnitude estimates only, because the actuators used in the investigation were not optimized for maximum effectiveness.

Acknowledgments

These efforts were sponsored by the Munitions Directorate of the U.S. Air Force Research Laboratory, U.S. Air Force Material Command, U.S. Air Force, under the direction of Chris Perry. The U.S. Government is authorized to reproduce and distribute reprints for governmental purposes notwithstanding any copyright notation thereon.

References

[1] Cadogan, D., Graham, W., and Smith, T., "Inflatable and Rigidizable Wings for Unmanned Aerial Vehicles," AIAA Paper 2003-6630, 2003.

[2] Cadogan, D., Smith, T., Uhelsky, F., and MacKusick, M., "Morphing Inflatable Wing Development for Compact Package Unmanned Aerial Vehicles," AIAA Paper 2004-1807, 2004.

[3] Post, M. L., and Corke, T. C., "Separation Control on High Angle of Attack Airfoil Using Plasma Actuators," *AIAA Journal*, Vol. 42, No. 11, 2004, pp. 2177–2184. doi:10.2514/1.2929

[4] Post, M. L., and Corke, T. C., "Flow Control with Single Dielectric Barrier Plasma Actuators," AIAA Paper 2005-4630, 2005.

[5] Corke, T. C., Jumper, E. J., Post, M. L., Orlov, D., and McLaughlin, T. E., "Application of Weakly Ionized Plasmas as Wing Flow-Control Devices," AIAA Paper 2002-0350, 2002.

[6] Hall, K. D., "Potential Flow Model for Plasma Actuation as a Lift Enhancement Device," M.Sc. Dissertation, Dept. of Aerospace and Mechanical Engineering, Univ. of Notre Dame, Notre Dame, IN, 2004.

[7] Hall, K. D., Jumper, E. J., Corke, T. C., and McLaughlin, T. E., "Potential Flow Model of a Plasma Actuator as a Lift Enhancement Device," AIAA Paper 2005-0783, 2005.

[8] Enloe, C. L., McLaughlin, T. E., VanDyken, R. D., Kachner, K. D., Jumper, E. J., and Corke, T. C., "Mechanisms and Responses of a Single Dielectric Barrier Plasma Actuator: Plasma Morphology," *AIAA Journal*, Vol. 42, No. 3, 2004, pp. 589–594. doi:10.2514/1.2305

[9] Enloe, C. L., McLaughlin, T. E., VanDyken, R. D., Kachner, K. D., Jumper, E. J., Corke, T. C., Post, M. L., and Haddad, O., "Mechanisms and Responses of a Single Dielectric Barrier Plasma Actuator: Geometric Effects," *AIAA Journal*, Vol. 42, No. 3, 2004, pp. 595–604. doi:10.2514/1.3884

[10] VanDyken, R. D., McLaughlin, T. E., and Enloe, C. L., "Parametric Investigations of a Single Dielectric Barrier Plasma Actuator," AIAA Paper 2004-46, 2004.

[11] Selig, M. S., Guglielmo, J. J., Broeren, A. P., and Giguere, P., *Summary of Low-Speed Airfoil Data*, SoarTech Publications, Virgina Beach, VA, Vol. 11995, , pp. 182–181.

[12] Mueller, T. J., and Batill, S. M., "Experimental Studies of Separation on a Two-Dimensional Airfoil at Low Reynolds Numbers," *AIAA Journal*, Vol. 20, No. 4, 1982, pp. 457–463.

[13] Moran, J., *An Introduction to Theoretical and Computational Aerodynamics*, Wiley, New York, 1984.

[14] Katz, J., and Plotkin, A., *Low-Speed Aerodynamics: From Wing Theory to Panel Methods*, 2nd ed., McGraw–Hill, New York, 1991.